The Astrophysical Journal, 752:43 (12pp), 2012 June 10 doi:10.1088/0004-637X/752/1/43

FORMATION OF MASSIVE BLACK HOLES IN DENSE STAR CLUSTERS. II. INITIAL MASS FUNCTION AND PRIMORDIAL MASS SEGREGATION

Sanghamitra Goswami[1], Stefan Umbreit[1], Matt Bierbaum[2], and Frederic A. Rasio[1,3]
[1] Department of Physics and Astronomy, Dearborn Observatory, Northwestern University, Evanston, IL 60208, USA
[2] Department of Physics, Clark Hall, Cornell University, Ithaca, NY 14853, USA
[3] Center for Interdisciplinary Exploration and Research in Astrophysics (CIERA), Northwestern University, Evanston, IL 60208, USA
Received 2011 May 29; accepted 2012 March 1; published 2012 May 24

ABSTRACT

A promising mechanism to form intermediate-mass black holes is the runaway merger in dense star clusters, where main-sequence stars collide and form a very massive star (VMS), which then collapses to a black hole (BH). In this paper, we study the effects of primordial mass segregation and the importance of the stellar initial mass function (IMF) on the runaway growth of VMSs using a dynamical Monte Carlo code for *N*-body systems with *N* as high as 10^6 stars. Our code now includes an explicit treatment of all stellar collisions. We place special emphasis on the possibility of top-heavy IMFs, as observed in some very young massive clusters. We find that both primordial mass segregation and the shape of the IMF affect the rate of core collapse of star clusters and thus the time of the runaway. When we include primordial mass segregation, we generally see a decrease in core-collapse time (t_{cc}). Although for smaller degrees of primordial mass segregation this decrease in t_{cc} is mostly due to the change in the density profile of the cluster, for highly mass-segregated (primordial) clusters, it is the increase in the average mass in the core which reduces the central relaxation time decreasing t_{cc}. The final mass of the VMS formed is always close to $\sim 10^{-3}$ of the total cluster mass, in agreement with previous studies and is reminiscent of the observed correlation between the central BH mass and the bulge mass of the galaxies. As the degree of primordial mass segregation is increased, the mass of the VMS increases at most by a factor of three. Flatter IMFs generally increase the average mass in the whole cluster, which increases t_{cc}. For the range of IMFs investigated in this paper, this increase in t_{cc} is to some degree balanced by stellar collisions, which accelerate core collapse. Thus, there is no significant change in t_{cc} for the somewhat flatter global IMFs observed in very young massive clusters.

Key words: galaxies: starburst – galaxies: star clusters: general – methods: numerical

Online-only material: color figures

1. INTRODUCTION

1.1. IMBHs

It is generally accepted that two separate classes of black holes (BHs) exist, defined by their mass ranges: stellar mass BHs of mass $\sim$3–20 $M_\odot$ (Bolton 1972; Webster & Murdin 1972; Casares 2007), which form through the collapse of massive stars, and supermassive BHs (SMBHs) of mass $\sim 10^6$–10^{10} $M_\odot$, which are found in the centers of most galaxies including the Milky Way (Kormendy & Gebhardt 2001; Merritt & Ferrarese 2001; Ghez et al. 2003; Miller & Colbert 2004). However, this leaves a gap in the mass range from $\sim 10^2$ to 10^4 $M_\odot$ which in recent years seems to have been filled by tentative evidence for intermediate-mass black holes (IMBHs; Portegies Zwart et al. 1999; Grindlay et al. 2001). This evidence consists of dynamical measurements (Gebhardt et al. 2002; Gerssen et al. 2002; van der Marel et al. 2002), detection of ultraluminous X-ray sources (ULX) found off-center in galaxies (Miller & Colbert 2004), the anomalously high mass-to-light ratio observed in the centers of some globular clusters (Miller & Colbert 2004), and the mass-segregation quenching in the cores of globular clusters in the presence of an IMBH (Pasquato et al. 2009).

The possible existence of IMBHs in globular clusters is suggested by the $M_{BH} - \sigma$ relation for galaxies, where M_{BH} is the mass of the central massive BH and σ is the velocity dispersion of the bulge. Extending this relation down to velocity dispersions typical for globular clusters ($\approx$10 km s^{-1}), we expect BH masses in the range of $\sim 10^3$–10^4 $M_\odot$. There are several claims in the literature that, indeed, such IMBHs are present in some globular clusters. The evidence is mainly based on measurements of the stellar velocity distribution, with velocity dispersions increasing strongly toward the center if an IMBH is present. The most promising candidates are the clusters G1 (Gebhardt et al. 2005, 2002) and ω Cen (Noyola et al. 2008). However, the presence of IMBHs in these clusters is still debated. For instance, based on scaled direct *N*-body models, Baumgardt et al. (2003) show that there is no need to invoke the presence of an IMBH in the center of G1 in order to explain the observed velocity dispersion profile. On the other hand, Gebhardt et al. (2005) point out that, since the region where the IMBH influences the velocity distribution is barely resolved, additional information from higher order velocity moments must be considered. Using orbit-based models to fit both surface brightness and velocity data simultaneously, they find (similar to their earlier results) that only these higher order velocity moments provide sufficient evidence for an IMBH in G1 with a mass of $1.8\,(\pm 0.5) \times 10^4\ M_\odot$. However, these results must still be confirmed using fully self-consistent evolutionary models that do not rely on assumed mass-to-light ratio profiles.

Numerous ULX sources have been identified by *Chandra* and *XMM-Newton*, often associated with starburst environments. These sources have X-ray luminosities of $L_X > 10^{39}$ erg^{-1}, exceeding the angle-averaged flux of a BH of mass $<20\,M_\odot$ accreting material at the Eddington luminosity, L_E. Although many ULX could be identified as active galactic nuclei at the centers of galaxies, and thus SMBHs, some are clearly off-center with typical projected distances of $\approx$400 pc (Miller & Colbert 2004). For instance, the ULX X41.4+60 in the starburst galaxy M82 (Portegies Zwart et al. 2004) has been found 7″ away from the galaxy center which corresponds to a distance of

≈200 pc. Kaaret et al. (2001) argue, therefore, that this X-ray source is unlikely to be an underluminous SMBH, as dynamical friction would cause it to spiral into the nucleus of the galaxy on timescales much shorter than the age of the galaxy. Based on this argument they derive an upper mass limit of $\approx 10^5\,M_\odot$. From the total X-ray luminosity and the assumption that the ULX source radiates isotropically at the Eddington rate, Kaaret et al. (2001) also derive a lower limit of $500\,M_\odot$. However, they point out that this value can be lower by a factor of a few when mild beaming is considered, thus bringing it closer to the stellar mass BH range. On the other hand, newer *Chandra* observations by Kaaret et al. (2009) have shown that during an outburst, where X41.4+60 increased its X-ray luminosity by a factor of more than three, its X-ray spectrum remained in the so-called hard state, characterized by a dominant power-law component containing 80% of the total flux (Remillard & McClintock 2006). From stellar mass BH X-ray binaries it is known that their spectra are in the hard state if $L < 0.3\,L_E$. If one assumes the same limit for higher-mass BH X-ray binaries, the peak luminosity of $8.5 \times 10^{40}\,\mathrm{erg}^{-1}$ inferred from *Chandra* observations would imply a lower-mass limit of $\approx 2000\,M_\odot$ (Kaaret et al. 2009). As one can see, even if one considers that the radiation could be mildly beamed, the minimum mass is well above the stellar mass BH range, making this source a prime IMBH candidate. Another good candidate for an IMBH is the recently found ULX source HLX-1 in the edge-on spiral galaxy ESO 243-49 (Farrell et al. 2009). With a maximum luminosity of up to $1.1 \times 10^{42}\,\mathrm{erg}^{-1}$ in the 0.2–10 kev band, and accounting for beaming effects, Farrell et al. (2009) obtain a conservative lower limit of $\sim 500\,M_\odot$.

Further indications for the presence of IMBHs in some globular clusters come from unusually high mass-to-light ratios measured in their centers, as inferred from pulsar timing measurements. For instance, the Galactic globular cluster NGC 6752 has five millisecond pulsars, three of which are in the core (D'Amico et al. 2002). Two of these three have negative period derivatives and one has an anomalously high positive period derivative. If the spin derivatives are due to the gravitational potential of the cluster, Ferraro et al. (2003) conclude that the mass-to-light ratio in the core is $M/L \approx 6$–7, much higher than that inferred for most globular clusters. For comparison, $M/L \approx 2$ is what one would expect for an old star cluster with a standard initial mass function (IMF) based on stellar evolution alone (Caputo 1985). Furthermore, based on the position of one of the pulsars, Ferraro et al. (2003) find that there is 1000–2000 $M_\odot$ of underluminous matter within the inner 0.08 pc of the cluster. This could be explained by a $\sim 1000\,M_\odot$ IMBH in the center of the cluster, but also by an exceptional concentration of dark remnants, or a $\sim 100\,M_\odot$ BH that is offset but near the projected location of the three millisecond pulsars in the cluster core. As the high spatial resolution in their observations does not show a cusp down to 0.08 pc, Ferraro et al. (2003) conclude that any central BH must have a mass $M \lesssim 1000\,M_\odot$.

There has been some considerable theoretical work by Gill et al. (2008) on observational evidences of IMBHs in star clusters. Mass segregation in star clusters brings heavier stars toward the center, increasing the average stellar mass in the core. As a diagnostic tool to quantify mass segregation, Gill et al. (2008) defined this radial variation of the average stellar mass as $\Delta m = \langle m \rangle_c - \langle m \rangle_{\rm rh}$, where Δm is the difference of the average mass in the core ($\langle m \rangle_c$) and the average mass at the projected half-mass radius of the cluster ($\langle m \rangle_{\rm rh}$). A cluster with no IMBH on a relaxation timescale settles to a quasi-equilibrium configuration with varying degrees of mass segregation (Δm). They found that in simulations of clusters with an IMBH, mass segregation (Δm) is significantly quenched. The idea is that, if there is an IMBH in the core, since the IMBH will be more massive than any of the other massive stars in the core, the IMBH has an extremely high probability of changing into a binary in a close three-body encounter. The subsequent interactions of this IMBH in a binary with other massive stars in the core might kick out or scatter the other massive stars in the core. Since the mass-segregated massive stars are the ones that will be scattered out of the core in this way, $\langle m \rangle_c$ will decrease. Thus, in a cluster with no central IMBH, mass segregation (Δm) will be more pronounced than in a cluster with an IMBH. According to the authors, this phenomenon of quenching mass segregation in the presence of an IMBH can be observed by high-resolution imaging of the cores of a large sample of globular clusters by the *Hubble Space Telescope* (Pasquato et al. 2009).

1.2. Pathways to IMBH Formation

There are several pathways discussed in the literature through which IMBHs may form. The simplest way is through the core collapse of a massive Population III star formed in a mini dark matter halo at high redshift (Madau & Rees 2001). At lower redshifts, such massive stars must be grown through mergers of lower-mass stars, which requires rather large stellar densities, typically $\geqslant 10^6\,\mathrm{pc}^{-3}$ (Freitag et al. 2006a; Ardi et al. 2008; Baumgardt et al. 2008). As an alternative to stellar mergers it is also possible to increase the mass of a stellar-mass BH by tidally disrupting and accreting other stars; however, this seems to require even larger stellar densities (Baumgardt et al. 2008).

In a cluster with a broad range of stellar masses, large stellar densities can be achieved through mass segregation, which will drive the most massive objects to the center, while lighter stars spread out to attain kinetic energy equipartition. However, for any reasonable IMF, the most massive stars are unable to achieve energy equipartition with the lighter stars and therefore decouple from the rest of the cluster and form a compact subsystem in the cluster center. This process is called Spitzer instability (Spitzer 1969) and causes core collapse to be accelerated (Spitzer 1969; Vishniac 1978; Watters et al. 2000; Gürkan et al. 2004). As shown by Gürkan et al. (2004, hereafter Paper I), for a realistically broad stellar mass spectrum, the core-collapse time ($t_{\rm cc}$) can be as short as $t_{\rm cc} = 0.15\,t_{\rm rc}(0)$, where $t_{\rm rc}(0)$ is the initial central relaxation time.

Once the most massive objects have segregated, the formation of an IMBH can occur in two different ways: one is when the massive stars have already evolved into stellar mass BHs at the time of core collapse and these BHs then merge by emitting gravitational waves. The BHs first form BH binaries which then harden through dynamical interactions with other objects until the binary is close enough for gravitational radiation to dissipate sufficient orbital energy until the BHs merge (see, e.g., O'Leary et al. 2006). However, growing an IMBH with a mass of $\sim 1000\,M_\odot$ through such stellar mass BH mergers is only realistic for the very massive clusters such as those in galactic nuclei (O'Leary et al. 2006). For smaller systems such as globular clusters, Mouri & Taniguchi (2002) and O'Leary et al. (2006) have shown that this mechanism is rather inefficient. This is because it is much more likely that the stellar mass BHs escape through strong dynamical binary interactions (Portegies Zwart & McMillan 2000) or recoil from asymmetric gravitational wave emission (Miller & Hamilton 2002; Gültekin et al. 2004; O'Leary et al. 2007) given the low cluster escape speed.

Another way to form an IMBH, which is not restricted to galactic nuclei, is through mergers of massive main-sequence stars that segregate to the center and drive cluster core collapse before the formation of stellar BHs. This subsystem of massive stars can enter a phase of rapid collisions, and since the most massive object has the largest cross-section for further collisions, this object is expected to grow in a runaway fashion. The resulting very massive star (VMS) eventually collapses to form an IMBH (Portegies Zwart & McMillan 2002; Gürkan et al. 2004). As the time it takes for the most massive stars to turn into BHs is approximately 3 Myr (Meynet & Maeder 2000), an IMBH is only formed through runaway merging if the cluster reaches core collapse within the first 3 Myr of dynamical evolution.

This simple picture has a few important caveats. First, the fate of such a massive merger remnant formed by a runaway is rather uncertain. Direct monolithic collapse to a BH with no or little mass loss is a possible outcome, at least for sufficiently small metallicities (Heger & Woosley 2002). However, it has been suggested that mass loss from stellar winds could dominate the mass increase due to repeated mergers (Glebbeek et al. 2009). In this case it might be difficult to form a VMS at all. On the other hand, within the runaway phase, it has been shown that, for clusters like those studied here, the time between collisions is much shorter than the Kelvin–Helmholtz timescale of the collision product, so that the growing VMS must be out of thermal equilibrium. Instead the calculations of Glebbeek et al. (2009) were done assuming that each merger remnant behaves exactly like an ordinary massive star in thermal equilibrium. The uncertainty in the final VMS (and IMBH) mass is further increased when considering that a stronger wind mass loss would also lead to a stronger expansion of the cluster core, decreasing the mass growth rate of the VMS by lowering the collision rate. To address this problem, one would need to perform a fully self-consistent simulation coupling the stellar dynamics with detail radiation hydrodynamics of the stellar collisions and mass loss from merger remnants. This is clearly beyond the scope of this paper.

The runaway collision scenario in globular clusters has been extensively investigated in Paper I and in Freitag et al. (2006a, 2006b) using Monte Carlo (MC) simulations for a large variety of initial conditions. Paper I focuses on the dependence of $t_{\rm cc}$ on the shape and the width of the IMF, the presence of a Galactic tidal field, and the cluster density profile. The key result is that for clusters with a broad range of masses, $t_{\rm cc}$ is set by the central relaxation time, $t_{\rm rc}(0)$, which means that for multi-mass clusters, core collapse depends on the local conditions in the core, while for single-mass clusters core collapse is a global phenomenon. Furthermore, it is clear that $t_{\rm cc}$ depends only weakly on the external tidal field. It was also found that the dependence of $t_{\rm cc}$ on the mass spectrum can be conveniently expressed by a single parameter $m_{\rm max}/\langle m\rangle$, where $m_{\rm max}$ is the maximum and $\langle m\rangle$ is the average stellar mass. For $m_{\rm max}/\langle m\rangle > 50$, the ratio $t_{\rm cc}/t_{\rm rc}$ converges to a constant value $\approx$0.15 for all IMFs and cluster density profiles. Combined with the requirement that $t_{\rm cc}$ be less than 3 Myr, this relation provides a uniform criterion for runaway growth to occur for a large range of possible, unsegregated cluster configurations.

Freitag et al. (2006a) performed similar simulations but also incorporating collisions explicitly. They quantified the dependence of the onset of the runaway on the initial collision time, and found that runaway growth happens earlier with respect to $t_{\rm rh}$, the half-mass relaxation time for initially more collisional clusters. Thus, collisions extend the parameter space of initial cluster conditions for runaway to occur. However, as pointed out by the authors, for any standard IMF (Kroupa, Salpeter, Miller-Scalo) this effect is negligible for masses typical for globular clusters. Thus, in this regime, the condition for runaway to occur reduces to the one found in Paper I, based on the central relaxation time alone.

The runaway collision scenario has also been verified numerically by direct N-body simulations. In Portegies Zwart & McMillan (2002), runaway collisions were produced in sufficiently dense and highly concentrated clusters with only a few 10^4 stars initially. Portegies Zwart et al. (2004) modeled the evolution of MGG-11 with $\approx 10^5$ and, in one case, with $\approx 5 \times 10^5$ stars, and found that, similar to Paper I, only clusters with a short enough mass-segregation timescale, or, correspondingly, low enough $t_{\rm rh}$, are likely to produce a runaway object. However, their results also show that, in addition to a short $t_{\rm rh}$, these clusters must also be sufficiently concentrated, corresponding to King models with $W_0 \geqslant 9$, in order to trigger a runaway object. This might be due to the fact that in the N-body simulations, binaries formed by three-body interactions (Freitag et al. 2006a), a process which is not included in the MC runs, and these binaries dominated the collisional evolution in the core. On the other hand, for $N \gtrsim 10^6$, Freitag et al. (2006a) have demonstrated that three-body binaries are of little importance for the collision process. Similarly, Portegies Zwart et al. (2004) find for their large $N \approx 5 \times 10^5$ run that the influence of three-body binaries on the collisional evolution is lower than in their lower-N runs. Thus, it appears that the nature of collisional runaway growth in a star cluster changes with increasing N from being less dominated by binary collisions and involving more and more single–single collisions.

Although the runaway merger scenario has been extensively investigated for a large variety of initial conditions, almost all of these studies started with unsegregated clusters, that is, clusters, where the stellar mass is not correlated with the radial position within the cluster. However, in recent years, observations frequently indicated that many young star clusters with ages of only a few Myr already show a strong degree of mass segregation, suggesting that mass segregation may be primordial and motivating a new study of its effects on collisional runaways.

1.3. Primordial Mass Segregation and Top-heavy IMF

Significant mass segregation has been found in many young star clusters. Mass segregation can be understood as the tendency toward equipartition of kinetic energies. This tendency for equipartition is a consequence of gravitational encounters, which attempt to drive the local velocity distribution toward a Maxwellian, with $m_1\langle V_1^2\rangle = m_2\langle V_2^2\rangle$ (Heggie & Hut 2003, Chapter 16). As a result, massive stars move more slowly, on average, than lighter ones, so the massive stars drop lower in the potential well, while the stars of smaller mass move out and may even escape (Heggie & Hut 2003, Chapter 16). This results in having the more massive members of a gravitationally bound system closer to the center whereas the lighter members are found further away. This dynamical mass segregation acts on a timescale of the order of the relaxation time of the cluster (Heggie & Hut 2003; Spitzer 1987, Section 4.2).

However, there are indications that the degree of mass segregation seen in many young clusters cannot be a result of their dynamical evolution as their ages are much less than their relaxation time (Hillenbrand 1997; Fischer et al. 1998; de Grijs

1998; Hillenbrand & Hartmann 1998; Gouliermis et al. 2004; Stolte et al. 2006). For instance, for NGC 330, the richest young star cluster in the Small Magellanic Cloud, observations show that the IMF becomes steeper at increasing distances from the cluster center, with the number of massive stars decreasing from the core to the outskirts of the cluster five times more rapidly than the less-massive objects, while the age of NGC 330 is 10 times shorter than the expected relaxation time of the cluster (Sirianni et al. 2002). Another example is provided by the Orion nebula cluster, in which it can be argued from numerical results that the massive stars in the center cannot have formed in the outer regions. This implies that the stellar mass is to some degree a function of the initial position within the cluster (Bonnell & Davies 1998). Interestingly, the 3 mm continuum observations obtained with the Combined Array for Research in Millimeter-Wave Astronomy of 11 Infrared Dark Cloud cores establish that the mass segregation can be identified at the formative stage of a stellar cluster (Perez Munoz & Carpenter 2007). All these observations suggest that many clusters may have been formed significantly mass-segregated.

Primordial mass segregation has been explained either by the formation of massive stars preferentially in the densest regions of the parent molecular cloud (Murray & Lin 1996) or by competitive gas accretion during the earliest phases of star formation (Bonnell & Bate 2006). An additional alternative has been suggested by McMillan et al. (2007). They show that a much higher degree of mass segregation in a cluster can be achieved if the cluster is a result of one or more mergers of smaller clusters. As the smaller clusters have shorter relaxation times, mass segregation proceeds faster. When the clusters merge, this larger degree of mass segregation is preserved in the final cluster.

Primordial mass segregation also has important consequences. It has been shown that, in an initially mass-segregated cluster, the effect of early mass loss due to stellar evolution is, in general, more destructive than for an unsegregated cluster with the same density profile, since this leads to shorter lifetimes, a faster initial evolution toward less concentrated structure, and a flattening of the stellar mass function (McMillan et al. 2008).

Recently, Ardi et al. (2008) studied the influence of initial mass segregation on the runaway growth of a massive star by means of direct N-body simulations of up to $\approx$131 stars. Contrary to the expectations from Gürkan et al. (2004), they found that, for a given density profile, initial mass segregation does not increase the available parameter space of cluster initial conditions leading to runaway growth. They argue that this is because the initial mass segregation *decreases* the collision rate of stars in the core as, due to the increased average mass, the number density is decreased. This is in line with earlier N-body simulations suggesting that runaway growth can occur only when the cluster is initially sufficiently collisional (Portegies Zwart et al. 2004), in contrast to predictions based only on the core-collapse time. This result should be tested for larger N as the nature of the collisional runaway changes from being dominated by three-body binary formation at low N to single–single collisions at high N.

One of the main uncertainties in star cluster evolution lies in determining the true IMF. Often it is assumed that the IMF is a standard power law (or power laws with different indices in different mass ranges) with no primordial radial variation in the cluster (e.g., Salpeter 1959; Miller & Scalo 1979; Kroupa 2001). Deviations from the standard IMFs are observed in many clusters both at the high- and low-mass ends (e.g., Elmegreen 2004). In particular, at the high-mass end, IMFs are observed to be generally flatter compared with the standard Salpeter power law in young massive clusters like the Arches cluster (Stolte et al. 2002; Kim et al. 2006).

2. NUMERICAL METHODS

2.1. Monte Carlo Code

The numerical method that has been used here to investigate the dynamical evolution of star clusters is the MC method, based on the classic work of Hénon (1971) and described in detail in Fregeau & Rasio (2007, and references therein). In MC simulations, N, the total number of stars in the cluster is dependent on the initial half-mass relaxation time in the cluster. For a Plummer sphere, it is given by (Spitzer 1987, Equation (2.63))

$$t_{\rm rh}(0) = \frac{0.138N}{\ln \gamma_c N}\left(\frac{r_h^3}{GM}\right)^{1/2}, \quad (1)$$

where $\gamma_c \sim 0.01$ is the Coulomb logarithm and r_h is the half-mass radius.

Since our code now includes an explicit treatment of all stellar collisions, we briefly summarize here the "sticky sphere" method for stellar collisions (Freitag & Benz 2002).

In the sticky sphere approximation, a collision occurs whenever the centers of two stars pass within a distance $d = (R_1+R_2)$, with $R_{1,2}$ being the stellar radii. Until this distance is reached, the gravitational influence of other stars as well as any mutual tidal interactions are neglected. The cross-section for such a collision is given by Binney & Tremaine (1987, Section 7.5.8),

$$S_{\rm coll}^{12} = \pi b_{\rm max}^2 = \pi(R_1+R_2)^2\left(1+\frac{(v_*^{12})^2}{v_{\rm rel}^2}\right), \quad (2)$$

where $b_{\rm max}$ is the largest impact parameter leading to contact, $v_{\rm rel}$ is the relative velocity between two stars, and $v_*^{12} = (2G(M_1+M_2)/(R_1+R_2))^{0.5}$. In a cluster where all stars have the same mass M_* and radius R_*, the average local collision time $T_{\rm coll}$ is given by Binney & Tremaine (1987, Section 7.5.8):

$$\frac{1}{T_{\rm coll}} = \frac{1}{n_*}\int d^3v_1 d^3v_2 f(v_1) f(v_2)||v_1 - v_2||S_{\rm coll}, \quad (3)$$

where n_* is the stellar number density. For a Maxwellian velocity distribution, this becomes

$$\frac{1}{T_{\rm coll}} = 16\sqrt{\pi} n_* \sigma_v R_*^2\left[1+\frac{GM_*}{2\sigma_v^2 R_*}\right], \quad (4)$$

where σ_v is the velocity dispersion.

In order to resolve collisional processes in an MC simulation, we constrain the time step size δt according to an estimate of the central collision time using

$$\delta t \leqslant f\tilde{T}_{\rm coll}, \quad (5)$$

where $f = 5\times10^{-3}$ is a constant chosen small enough to ensure that collisions are sampled sufficiently and $\tilde{T}_{\rm coll}$ is an estimate of $T_{\rm coll}$ based on Equation (4) and given by

$$\frac{1}{\tilde{T}_{\rm coll}} = 16\sqrt{\pi} n_* \sigma_v \left\langle R_*^2\right\rangle\left[1+\frac{G\left\langle M_* R_*\right\rangle}{2\sigma_v^2\left\langle R_*^2\right\rangle}\right], \quad (6)$$

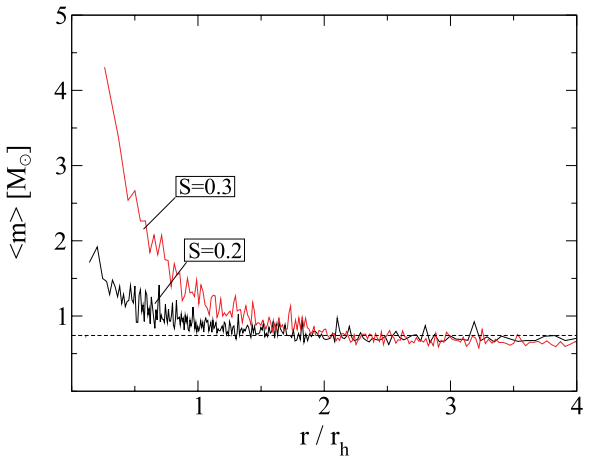

Figure 1. Average stellar mass profile for initially mass-segregated clusters created according to the prescription of Šubr et al. (2008). All the simulations shown here contain 5×10^5 stars with a Salpeter IMF (within $M_{\rm min} = 0.2\,M_\odot$ and $M_{\rm max} = 120\,M_\odot$). The horizontal axis shows the cluster radius in units of the initial half-mass radius. The dotted straight line is for an initially unsegregated cluster and the red and black solid straight lines are for clusters with different degrees of primordial mass segregation ($S = 0.3, 0.2$). The average mass for the mass-segregated clusters increases steeply within $\sim 1\,r_{\rm h}$. For $S = 0.3$, the increase is by up to a factor of $\sim$5.

(A color version of this figure is available in the online journal.)

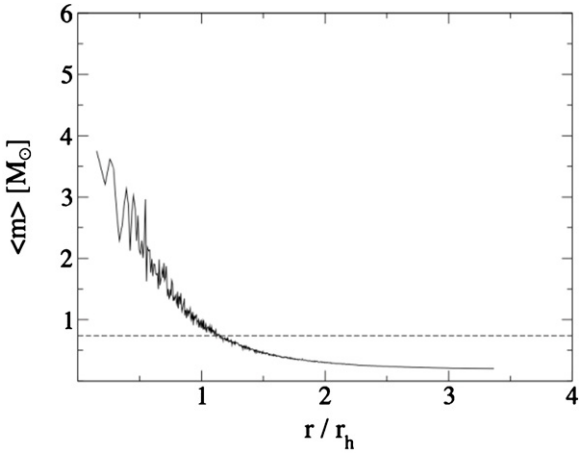

Figure 2. Same as Figure 1 but the primordially mass-segregated cluster is generated using the Baumgardt et al. (2008) recipe. Even in this case the average stellar mass of the cluster rises strongly within $1\,r_{\rm h}$, by up to a factor of $\sim$5.

with quantities in angular brackets being local averages. The collision probability for two neighboring stars is calculated as

$$P_{\rm coll} = n_* v_{\rm rel} S_{\rm coll} \delta t, \qquad (7)$$

where n_* is a local estimate of the stellar number density. The time step size δt is chosen such that $P_{\rm coll} \ll 1$. A random number (between 0 and 1) is then drawn. If the random number $< P_{\rm coll}$, two stars are selected for a collision and they are merged under the assumption of mass and linear momentum conservation.

The units adopted for our simulations are the standard N-body units of the MC code, and the same as in Paper I.

2.2. Implementation of Primordial Mass Segregation and Top-heavy IMFs

The effect of primordial mass segregation was studied in Paper I using a preliminary prescription. However, the recipe in Paper I is not defined with well-constrained parameters. In this paper, we have used recipes that are more realistically modeled and we do a much more extensive study.

Here, we consider two prescriptions for mass segregation: (1) the prescription of Šubr et al. (2008) for generating mass-segregated clusters, in which the degree of mass segregation can be adjusted by a parameter S related to the mean inter-particle energy of the stars and (2) the Baumgardt et al. (2008) prescription, which creates a maximally mass-segregated cluster in virial equilibrium.

From N-body models, Šubr et al. (2008) find that the quantity that is transferred between the light and massive stars is the potential energy, while their average kinetic energy remains nearly constant during the cluster evolution. Therefore, mass segregation is generated in terms of mean inter-particle potentials $\langle U^{ij} \rangle$, which is parameterized as

$$\langle U^{ij} \rangle = 2(1-S)^2 \langle U_{\rm tot} \rangle \frac{M_{*i} M_{*j}}{M_{\rm tot}^2} \left(\frac{M_{\rm sub}^i M_{\rm sub}^j}{M_{\rm tot}^2} \right)^{-S}, \qquad (8)$$

where M_{*i} and M_{*j} denote the masses of the ith and jth particle, $M_{\rm tot}$ denotes the total mass of the cluster, $U_{\rm tot}$ is the total potential energy of the cluster, $M_{\rm sub}^{i,j}$ is the sum of all $M_{*k} < M_{*i,j}$, and S is the degree of mass segregation which can have values between 0 and 1 (for a detailed description of the code refer to Šubr et al. 2008). In this recipe, $S = 0$ implies an unsegregated cluster and $S = 1$ a completely mass-segregated cluster. Relating to entropy, $S = 0$ has the lowest entropy and the system is highly symmetric in terms of $\langle U^{ij} \rangle$, while for $S = 1$, all the binding energy is carried by the two most massive stars in the cluster and corresponds to a state of maximum entropy. With this parameterization of the inter-particle potential, quasi-stationary, star-by-star realizations of mass-segregated clusters are generated. The stars are assigned masses according to the Salpeter IMF with maximum and minimum mass of $0.2\,M_\odot$ and $120\,M_\odot$, respectively.

An important property of this mass-segregation recipe is that both the density profile and the average mass in the core ($\langle m \rangle_c$) is different for each value of S, starting from a Plummer sphere for $S = 0$. This has the consequence that $t_{\rm rc}(0)$ which is dependent on density in the core (ρ_c) and $\langle m \rangle_c$ changes. This in turn causes $t_{\rm cc}$ to change.

The recipe from Baumgardt et al. (2008), on the other hand, does not change the underlying density profile and generates mass-segregated clusters, in comparison, much faster. It essentially sorts all stars such that, for a given density profile, the most massive stars have, on average, the lowest specific total energy.

Figures 1 and 2 show the average mass profile for the initially mass-segregated clusters (and unsegregated clusters also for comparison) using the Šubr et al. (2008) and Baumgardt et al. (2008) recipes, respectively. As can be seen in these plots, the average mass rises rapidly within one half-mass radius, by up to a factor of $\sim$5 (for the Baumgardt et al. 2008 recipe as well as for $S = 0.3$) for the initially mass-segregated clusters. Similarly, Figures 3 and 4 show the enclosed mass for the same two prescriptions. Comparing the median positions of the massive stars in these models, it becomes clear that the massive stars are on average at much smaller radii in initially mass-segregated clusters compared with non-segregated ones, as expected. The median distance from the cluster center can be up to a factor of $\simeq$4 smaller for stars with masses larger than $50\,M_\odot$. Comparing the enclosed stellar mass profiles for the two recipes

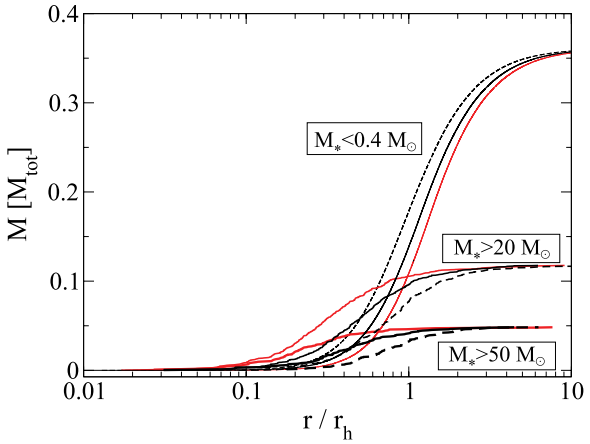

Figure 3. Enclosed stellar mass in primordially mass-segregated (solid lines) and unsegregated (dashed lines) clusters. The average mass in the cluster is ≈0.68 $M_\odot$. The black and red solid lines are for mass-segregated clusters (Šubr et al. 2008 recipe) with the degree of mass segregation, $S = 0.2$ and $S = 0.3$, respectively. We show here mass enclosed in stars more massive than the average mass of the cluster ($M_* > 20\,M_\odot$ and $M_* > 50\,M_\odot$) as well as mass enclosed in stars of mass less than the average mass ($M_* < 0.4\,M_\odot$). All the simulations shown here contain 5×10^5 stars with a Salpeter IMF (within $M_{\rm min} = 0.2\,M_\odot$ and $M_{\rm max} = 120\,M_\odot$). Lines denoting enclosed stellar mass contained in stars more massive than the average mass (i.e., $M_* > 20\,M_\odot$ and $M_* > 50\,M_\odot$) show that the massive stars in the unsegregated clusters are at significantly larger radii than the primordially mass-segregated cluster. The median position of massive stars in the unsegregated cluster differs by a factor of ∼4 for stars with $M_* > 50\,M_\odot$, and by a factor of ∼3 for stars with $M_* > 20\,M_\odot$, compared with the mass-segregated cluster with $S = 0.3$. Whereas lines denoting enclosed stellar mass contained in stars less massive than the average mass (i.e., $M_* < 0.4\,M_\odot$) show that the low-mass stars are definitely much more spread out in the case of primordially mass-segregated clusters when compared with the unsegregated cluster.

(A color version of this figure is available in the online journal.)

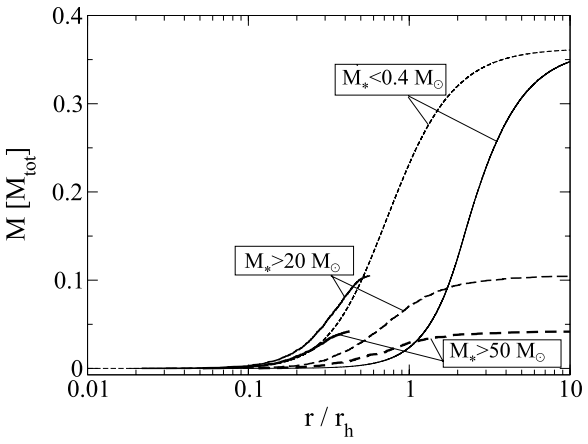

Figure 4. Same as Figure 3 but for primordially mass-segregated clusters using the Baumgardt et al. (2008) recipe. The black solid lines denote the primordially mass-segregated clusters and the dashed lines are for unsegregated clusters. Massive stars in unsegregated clusters are at significantly larger radii, with their median position differing by a factor of ∼4 for stars with $M_* > 50\,M_\odot$, and by a factor of ∼3 for stars with $M_* > 20\,M_\odot$, compared with the primordially mass-segregated clusters.

Table 1
Classification of IMF

IMF	Range of m ($M_\odot$)	α
Kroupa		
	0.1–0.5	−1.3
	0.5–∞	−2.3
Arches		
	0.1–0.5	−1.3
	0.5–1.0	−2.3
	1.0–3.0	−2.04
	3.0–15.0	−1.5
	15.0–∞	−1.72
Variable		
	0.1–0.5	−1.3
	0.5–1.0	−2.3
	1.0–3.0	−2.04
	3.0–∞	−1.72

(Figures 3 and 4), it can be seen that the Baumgardt et al. (2008) recipe agrees pretty closely with the Šubr et al. (2008) recipe for $S = 0.3$.

In this paper, we also study the effect of flatter IMFs on the runaway collision scenario in young massive star clusters. We introduce a new IMF in this paper motivated by the Arches IMF from Dib et al. (2007). For the rest of the paper, this new IMF will be called the "Variable IMF," and we will denote the sections of this IMF ($dN/dm \propto m^{-\alpha}$) as $[\alpha_1 \ldots \alpha_4]$ with α_4 corresponding to the high-mass tail of the IMF. This Variable IMF is a variation on the Arches IMF (Dib et al. 2007) by leaving out the middle section from 3.0–15.0 $M_\odot$ so that the IMF is then more easily compared with the standard Kroupa IMF. The upper mass section of the Variable IMF is much flatter than traditional Salpeter (1955), Kroupa (2002), or Miller & Scalo (1979) IMFs. We therefore expect a greater number of high-mass stars, increasing both the average mass as well as the entire cluster mass.

2.3. Initial Conditions

For all the simulations in this paper, our code includes physical processes such as two-body relaxation and physical stellar collisions between stars in the "sticky sphere" approximation. In this paper, we do not include stellar evolution in our calculations since our aim here is to investigate dynamical processes taking place before even the most massive main-sequence stars in the cluster have evolved (i.e., <3 Myr). We have also not included any primordial binaries in our simulations just to keep the simple picture of runaway in the presence of primordial mass segregation, and exclude the effects of primordial binaries on runaway collisions (Gürkan et al. 2006).

The most important physical properties of all our initial cluster models are given in Tables 2 and 3. A comparison of the Variable IMF with the Arches IMF or with the standard Kroupa IMF is given in Table 1. In Table 2, we have listed simulations of clusters with the Variable IMF, varying α_3 and α_4. We have also listed the simulations done with the Salpeter IMF varying $M_{\rm max}$. In all these simulations, our focus has been to investigate the effect of IMF on the core collapse of young massive clusters. All our models start with an isolated Plummer sphere and the virial radius has been chosen such that the corresponding cluster has a core-collapse time of 3 Myr.

In Table 3, we have listed simulations of clusters for different values of initial N and initial virial radius, $r_{\rm vir}$, varying the degree of primordial mass segregation. Virial radius is defined by

$$r_{\rm vir} = -\frac{GM^2}{4E}, \tag{9}$$

where M is the total mass and E is the total gravitational energy of the cluster. This grid formed by the different values of initial

Table 2
Initial Conditions and Results for Simulations with Varying IMF

Name	IMF	r_{vir} (pc)	t_{cc}/t_{rh}
01	Variable $\alpha_3 = -2.04, \alpha_4 = -1.7$	0.39	0.127
02	Variable $\alpha_3 = -2.04, \alpha_4 = -1.8$	0.39	0.103
03	Variable $\alpha_3 = -2.04, \alpha_4 = -1.9$	0.39	0.092
04	Variable $\alpha_3 = -2.04, \alpha_4 = -2.0$	0.39	0.088
05	Variable $\alpha_3 = -2.04, \alpha_4 = -2.1$	0.39	0.077
06	Variable $\alpha_3 = -2.04, \alpha_4 = -2.2$	0.39	0.081
07	Variable $\alpha_3 = -2.04, \alpha_4 = -2.3$	0.39	0.078
08	Variable $\alpha_3 = -1.9, \alpha_4 = -1.72$	0.39	0.132
09	Variable $\alpha_3 = -2.0, \alpha_4 = -1.72$	0.39	0.125
10	Variable $\alpha_3 = -2.1, \alpha_4 = -1.72$	0.39	0.117
11	Variable $\alpha_3 = -2.2, \alpha_4 = -1.72$	0.39	0.102
12	Variable $\alpha_3 = -2.3, \alpha_4 = -1.72$	0.39	0.099
13	Salpeter $M_{max} = 110$	0.39	0.067
14	Salpeter $M_{max} = 100$	0.39	0.073
15	Salpeter $M_{max} = 90$	0.39	0.0812
16	Salpeter $M_{max} = 80$	0.39	0.079
17	Salpeter $M_{max} = 70$	0.39	0.097
18	Salpeter $M_{max} = 60$	0.39	0.108

Notes. r_{vir} is the virial radius of the cluster, t_{cc} denotes the core-collapse time of the cluster, and t_{rh} denotes the half-mass relaxation time. All models start as Plummer spheres with $N = 5 \times 10^5$ and the Variable IMF covers the same mass range (0.2–120 $M_\odot$).

N and initial r_{vir} is referred to as the parameter space in the later part of the paper. For all the simulations listed here, our aim has been to investigate the effect of primordial mass segregation on t_{cc} of young clusters with different initial conditions (N and r_{vir}). We have calculated t_{cc} based on the central relaxation time t_{rc} defined as

$$t_{rc}(0) = \frac{\sigma_c^3}{4.88\pi G^2 (\ln \gamma_c N) n \langle m \rangle_c^2}, \quad (10)$$

where σ_c, n, and $\langle m \rangle_c$ are the three-dimensional velocity dispersion, the number density, and the average stellar mass, respectively, at the cluster center (Spitzer 1987, Equation (3.37)). As a typical reference model similar to Paper I, all the simulations in Table 3 are initiated with Plummer models and the Salpeter IMF (within $M_{min} = 0.2\,M_\odot$ and $M_{max} = 120\,M_\odot$). Another reason for using Plummer sphere is that the Šubr et al. (2008) formalism starts with an isolated Plummer sphere.

3. RESULTS

3.1. Primordial Mass Segregation

Freitag et al. (2006a) were the first to study the core collapse and collisional runaway for unsegregated clusters using an MC simulation code including stellar collisions. Similar to Freitag et al. (2006a), we did not take into account the stellar evolution in the simulations since all the simulations were limited to the first 3 Myr, before the most massive stars lose mass in supernova explosions. If a cluster had a core-collapse time more than 3 Myr, we implicitly took stellar evolution into account by ending the simulation at 3 Myr. Since our code now includes stellar collisions, we first checked whether we are able to reproduce their results. They found that for all models with $t_{rc} < 20$ Myr, runaway formation of a VMS occurred.

Figure 5 is a parameter survey similar to Freitag et al. (2006a, their Figure 1), showing for each simulation whether

Table 3
Initial Conditions and Results of Simulations with Primordial-Mass Segregation (Šubr Recipe)

Name	N	r_{vir} (pc)	S	$t_{rc}(0)$ (Myr)	t_{cc} (Myr)
1a	3×10^5	0.50	0.00	29.30	4.40
1b	3×10^5	0.50	0.05	21.86	3.28
1c	3×10^5	0.50	0.10	19.33	2.90
1d	3×10^5	0.50	0.20	11.26	1.69
1e	3×10^5	0.50	0.30	6.80	1.02
2a	3×10^5	0.62	0.00	28.66	4.30
2b	3×10^5	0.62	0.05	24.53	3.68
2c	3×10^5	0.62	0.10	13.00	1.95
2d	3×10^5	0.62	0.20	10.33	1.55
2e	3×10^5	0.62	0.30	5.86	0.88
3a	3×10^5	0.77	0.00	41.33	6.20
3b	3×10^5	0.77	0.05	31.53	4.73
3c	3×10^5	0.77	0.10	20.80	3.12
3d	3×10^5	0.77	0.20	19.20	2.88
3fe	3×10^5	0.77	0.30	13.93	2.09
5a	5×10^5	0.41	0.00	25.86	3.88
5b	5×10^5	0.41	0.05	21.13	3.17
5c	5×10^5	0.41	0.10	17.4	2.61
5d	5×10^5	0.41	0.15	10.00	1.50
5e	5×10^5	0.41	0.20	8.66	1.30
5f	5×10^5	0.41	0.25	8.0	1.20
5g	5×10^5	0.41	0.30	5.53	0.83
6a	5×10^5	0.52	0.00	31.86	4.78
6b	5×10^5	0.52	0.05	22.53	3.38
6c	5×10^5	0.52	0.10	13.93	2.09
6d	5×10^5	0.52	0.15	14.13	2.12
6e	5×10^5	0.52	0.20	10.46	1.57
6f	5×10^5	0.52	0.25	10.53	1.58
6g	5×10^5	0.52	0.30	9.93	1.49
7a	5×10^5	0.64	0.00	38.66	5.80
7b	5×10^5	0.64	0.05	23.33	3.50
7c	5×10^5	0.64	0.10	16.66	2.50
7d	5×10^5	0.64	0.15	17.53	2.63
7e	5×10^5	0.64	0.20	16.00	2.40
7f	5×10^5	0.64	0.25	16.00	2.40
7g	5×10^5	0.64	0.30	13.53	2.03
7h	5×10^5	0.64	0.00	38.33	5.75
7i	5×10^5	0.64	0.05	23.33	3.50
7j	5×10^5	0.64	0.10	15.93	2.39
7k	5×10^5	0.64	0.15	17.86	2.68
7l	5×10^5	0.64	0.20	16.00	2.40
7m	5×10^5	0.64	0.25	15.93	2.39
7n	5×10^5	0.64	0.30	14.00	2.10
7o	5×10^5	0.64	0.00	38.66	5.80
7p	5×10^5	0.64	0.05	25.33	3.80
7q	5×10^5	0.64	0.10	16.66	2.50
7r	5×10^5	0.64	0.15	10.76	2.69
7s	5×10^5	0.64	0.20	16.00	2.40
7t	5×10^5	0.64	0.25	16.00	2.40
7u	5×10^5	0.64	0.30	14.06	2.11
7v	5×10^5	0.64	0.00	40.00	6.00
7x	5×10^5	0.64	0.05	23.33	3.50
7w	5×10^5	0.64	0.10	16.86	2.53
7y	5×10^5	0.64	0.15	17.53	2.63
7z1	5×10^5	0.64	0.20	16.00	2.40
7z2	5×10^5	0.64	0.25	16.00	2.40
7z3	5×10^5	0.64	0.30	13.33	2.00
8a	5×10^5	0.77	0.00	52.60	7.89
8b	5×10^5	0.77	0.05	34.60	5.19
8c	5×10^5	0.77	0.10	28.26	4.24
8d	5×10^5	0.77	0.15	24.20	3.63
8e	5×10^5	0.77	0.20	20.40	3.06
8f	5×10^5	0.77	0.25	19.73	2.96

Table 3
(Continued)

Name	N	r_{vir} (pc)	S	$t_{rc}(0)$ (Myr)	t_{cc} (Myr)
8g	5×10^5	0.77	0.30	16.53	2.48
9a	1×10^6	0.41	0.10	20.8	3.12
9b	1×10^6	0.41	0.15	19.06	2.86
9c	1×10^6	0.41	0.20	16.53	2.48
9d	1×10^6	0.41	0.30	10.40	1.56
10a	1×10^6	0.51	0.10	32.60	4.89
10b	1×10^6	0.51	0.15	21.46	3.22
10c	1×10^6	0.51	0.20	17.66	2.65
10d	1×10^6	0.51	0.30	15.53	2.33
11a	1×10^6	0.83	0.10	46.53	6.98
11b	1×10^6	0.83	0.15	43.73	6.56
11c	1×10^6	0.83	0.20	27.60	4.24
11d	1×10^6	0.83	0.30	20.06	3.01
12a	1×10^6	1.10	0.10	60.53	9.08
12b	1×10^6	1.10	0.15	59.26	8.89
12c	1×10^6	1.10	0.20	52.40	7.86
12d	1×10^6	1.10	0.30	44.46	6.67

Notes. Here N and r_{vir} are the initial number of stars and the initial virial radius, respectively. S is the degree of mass segregation (Equation (8)), $t_{rc}(0)$ is the initial central relaxation time, and t_{cc} denotes the core-collapse time. All initial models are isolated Plummer spheres with standard Salpeter IMFs with a mass range (0.2–120 $M_\odot$). Calculation of t_{rc} and t_{cc}: for Plummer models $r_v = 1$ and $r_h = 0.769$ in N-body units (Paper I, their Table 1). From r_v in physical units we calculate r_h in physical units. With initial N and initial r_h (in physical units) we also calculate the initial half-mass relaxation time in physical units, given by $t_{rh} = (0.138N/\ln \gamma N)\times(r_h^3/GM)^{1/2}$. From t_{rh}, we calculate t_{rc} (t_{rh} and t_{rc} for Plummer models is 0.093 and 0.0437, respectively, in Fokker–Planck units). Finally, we obtain $t_{cc} = 0.15\, t_{rc}$.

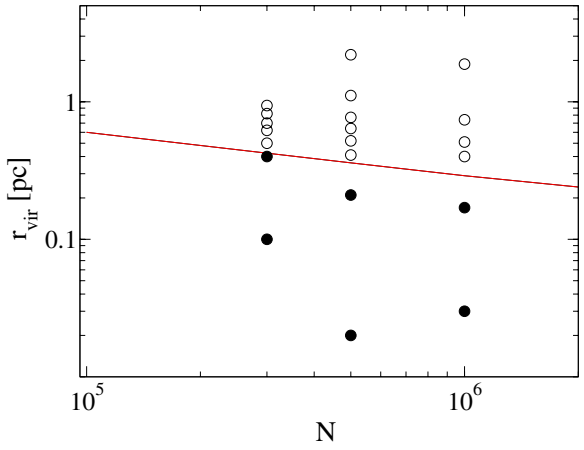

Figure 5. Parameter space survey for the primordially unsegregated clusters. All the simulations shown here contain 5×10^5 stars with a Salpeter IMF (within $M_{min} = 0.2\, M_\odot$ and $M_{max} = 120\, M_\odot$). Each circle represents a simulation of a cluster with a particular virial radius (r_{vir}) and number of stars (N). Filled circles represent simulations that result in a runaway while the empty circles indicate cases in which no runaway occurs. The straight line denotes $t_{cc} = 0.15\, t_{rc} = 3$ Myr as a function of r_{vir} and N; clusters with initial conditions below this line have $t_{cc} < 3$ Myr. As expected, we see in this plot that all the simulations that result in a runaway do in fact fall below this line.

(A color version of this figure is available in the online journal.)

a runaway occurred (filled circles) or not (open circles), for all our unsegregated models varying r_{vir} and the number of stars in the cluster. The solid straight line corresponds to $t_{cc} = 0.15\, t_{rc} = 3$ Myr, not including collisions. Simulations of clusters with initial conditions lying below the straight line will have $t_{cc} < 3$ Myr, whereas $t_{cc} > 3$ Myr for simulations with

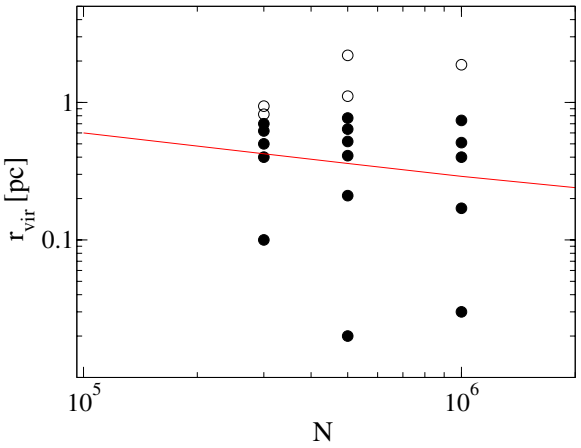

Figure 6. Same as Figure 5 but all the simulations are for primordially mass-segregated clusters ($S = 0.3$). The solid straight line once again denotes $t_{cc} = 0.15\, t_{rc} = 3$ Myr as a function of r_{vir} and N for initially unsegregated clusters. This plot shows that simulations of primordially mass-segregated clusters with initial conditions even above the solid straight line might have core-collapse time less than 3 Myr and can result in a runaway. Thus, simulations of primordially mass-segregated clusters increase the parameter space (range of r_{vir} in pc) for runaway collisions to happen when compared with simulations of primordially unsegregated clusters by at least a factor of ≈3.

(A color version of this figure is available in the online journal.)

initial conditions above the line. It can be clearly seen in Figure 5 that the initial conditions leading to a runaway indeed fall below this line. Thus, we have successfully reproduced the results of Freitag et al. (2006a) with our code and have reconfirmed the validity of the simple criterion for runaway collisions to occur in young dense star clusters.

We then repeated the same set of simulations for primordially mass-segregated clusters using the recipe from Šubr et al. (2008) with $S > 0$. Figure 6 shows our results for mass-segregation parameter $S = 0.30$. We see that, with primordial mass segregation, the initial cluster r_{vir} can be chosen several times larger compared with unsegregated clusters and still lead to a runaway. Thus, simulations of primordially mass-segregated clusters increase the parameter space (range of r_{vir} in pc) for runaway collisions to happen when compared with simulations of primordially unsegregated clusters.

To further illustrate the effect primordial mass segregation has on the mass growth of the most massive star, we compared results of a primordially mass-segregated versus an unsegregated cluster, with otherwise identical initial conditions. Figure 7 shows the growth curve of the most massive star in an unsegregated cluster and in a primordially mass-segregated cluster ($S = 0.3$), with $N = 5 \times 10^5$ stars and $r_{vir} = 0.64$ pc. The unsegregated cluster does not have a runaway or a very steep mass growth before it reaches core collapse, and only a 200 $M_\odot$ star is formed within 3 Myr. For the primordially mass-segregated cluster, we clearly see a very steep mass growth leading to a formation of a 900 $M_\odot$ star within 3 Myr and hence a runaway. A general result, in agreement with Freitag et al. (2006a), is that only one VMS forms in the cluster and there is no sign of multiple runaways. Note that this result might be different for clusters with significant fractions of primordial binaries (Gürkan et al. 2006). As in this example, we also note in all our simulations that the time of the runaway coincides with the time of core collapse, which decreases from $t_{cc} \sim 6$ Myr for the unsegregated cluster, and to $t_{cc} \sim 2$ Myr for the primordially mass-segregated cluster.

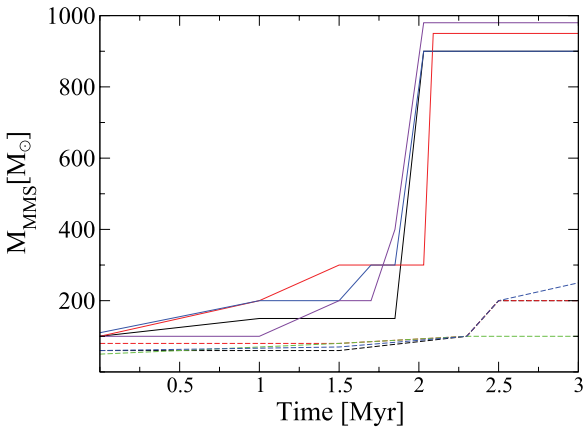

Figure 7. Growth curves of the most massive star (M_{MMS}) of an unsegregated cluster (dashed lines) and primordially mass-segregated cluster (solid lines) with $N = 5 \times 10^5$ stars and virial radii of 0.64 pc. The different colors indicate simulations of the same cluster with different random seeds. While the most massive star in the primordially mass-segregated cluster has a very steep and rapid mass growth leading to a runaway, the most massive star in the unsegregated cluster shows no such effect. For the unsegregated cluster $t_{rc} = 38.67$ (red), 38.33 (blue), 38.66 (green), and 40 Myr (purple) while for the primordially mass-segregated cluster t_{rc} values are 13.53 (red), 14.0 (blue), 14.0 (green), and 13.33 Myr (purple).

(A color version of this figure is available in the online journal.)

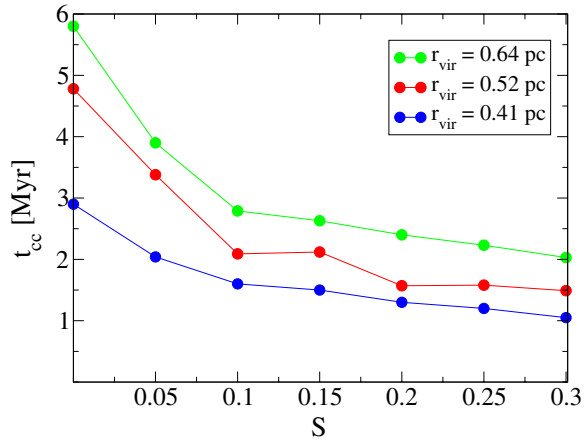

Figure 8. Decrease in the core-collapse time (t_{cc}) of a cluster with $N = 5 \times 10^5$ stars, as the degree of primordial mass segregation (S) is increased in the cluster. For each value of S, the three different colors represent simulations with three different virial radii (r_{vir}).

(A color version of this figure is available in the online journal.)

To show how strongly the core-collapse time decreases for other values of S, we plot in Figure 8 the core-collapse time for clusters with different initial r_{vir}, against S. We clearly see a trend of decreasing t_{cc} with increasing S. The decrease in t_{cc} is steepest for $S \lesssim 0.1$, causing a reduction of t_{cc} by a factor of $\approx$2. For $S > 0.1$, the decrease in t_{cc} is weaker, reducing t_{cc} by another 30%. This trend is also illustrated in Table 3 where we have shown that t_{cc} decreases for simulations with primordial mass segregation, when compared with the simulations of initially unsegregated clusters with similar initial conditions.

To analyze this trend further, we first check whether the simple relation from Paper I between t_{cc} and $t_{rc}(0)$ ($t_{cc}/t_{rc}(0) = 0.15$) remains still valid for mass-segregated clusters. In Figure 9, we plot t_{cc}/t_{rc} against S for clusters with different r_{vir}. We see that t_{cc}/t_{rc} remains nearly constant at 0.15 with only a $\sim$10% scatter. Thus, we conclude that the ratio of t_{cc}/t_{rc} remains consistent

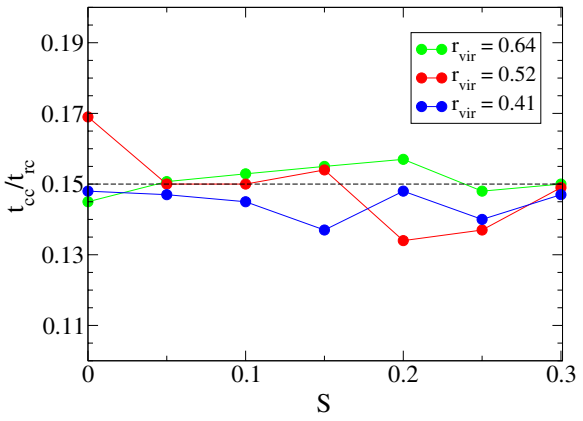

Figure 9. Dependence of core-collapse time in units of the central relaxation time, on primordial mass segregation (S). For each value of S, the three different colors represent simulations with three different virial radii (r_{vir}). For comparison, t_{cc}/t_{rc} as predicted in Paper I for unsegregated clusters is plotted as the dotted line. Even for the mass-segregated clusters t_{cc}/t_{rc} remains roughly consistent with Paper I.

(A color version of this figure is available in the online journal.)

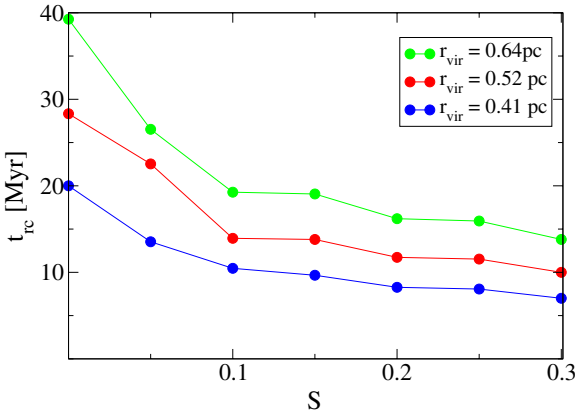

Figure 10. Decrease in the central relaxation time (t_{rc} in Myr) of a cluster of 5×10^5 stars with the increase in the degree of primordial mass segregation (S). For each value of S, the three different colors represent simulations with three different virial radii (r_{vir}).

(A color version of this figure is available in the online journal.)

with the value found in Paper I and the strongly decreasing t_{cc} can then only be caused by a decrease in $t_{rc}(0)$. This is also shown in Figure 10, where we plot $t_{rc}(0)$ against S for clusters with different r_{vir}. We notice a very similar decrease in t_{rc} as in t_{cc}, with increasing S, so the reason for the shorter t_{cc} must be attributed to shorter t_{rc}.

However, in the Šubr et al. (2008) formulation it is not a priori clear whether this decrease in t_{rc} is entirely related to an increase in primordial mass segregation, as the central density (ρ_c) also increases with S (Section 4.2). In order to disentangle these effects, we calculate relative contributions of all the factors to t_{rc}. We note that $t_{rc} \propto \sigma_c^3/\rho_c \langle m \rangle_c$, where σ_c is the velocity dispersion in the core and $\langle m \rangle_c$ is the average stellar mass in the core. Figure 11 plots the variation of σ_c^3, $1/\rho_c$, and $1/\langle m \rangle_c$, normalized to their values at $S = 0$, against S in a cluster with $N = 5 \times 10^5$ stars. The inverse of the normalized initial central density of the clusters decreases as S is increased from 0.0 to 0.15 by 25%, and then remains nearly constant for larger S values. The inverse of normalized $\langle m \rangle_c$ in the cluster always decreases with the increase in mass segregation, up to a factor of 2.5 for $S = 0.3$. The variation of σ_c^3, on the other hand, is only

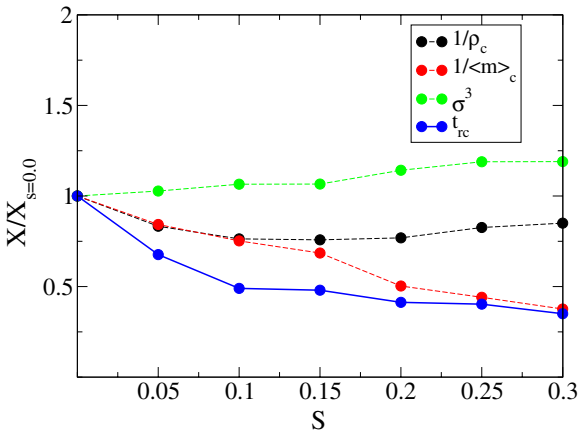

Figure 11. Evolution of the central relaxation time t_{rc} (solid line) and the factors affecting t_{rc} (dotted lines). All parameters are normalized to their values for an unsegregated cluster, $(X/X_{S=0.0})$. The black line is for the inverse of central density $(1/\rho_c)$, the intermediate gray is for the inverse of average stellar mass in the core $(1/\langle m\rangle_c)$, and the light gray represents the cube of the velocity dispersion in the core (σ_c^3). While σ_c^3 remains almost the same with increasing S, both $1/\rho_c$ and $1/\langle m\rangle_c$ decrease t_{rc}. However, for higher values of S ($S > 0.15$), it is mainly $1/\langle m\rangle_c$ which decreases t_{rc}.

(A color version of this figure is available in the online journal.)

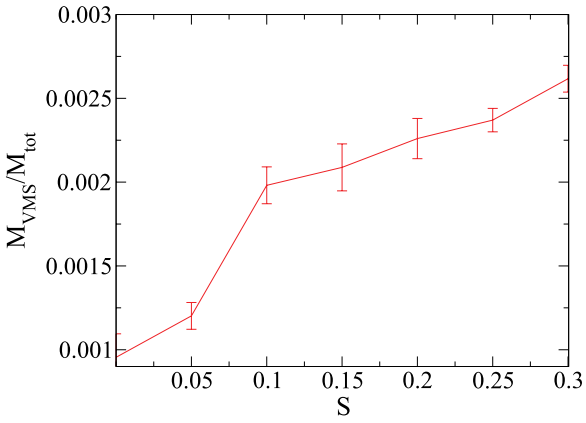

Figure 12. Fraction of the total stellar mass in the cluster, that ends up as a VMS after a runaway collision, as a function of the degree of mass segregation. All the simulations are for a cluster of 5×10^5 stars and a virial radius of 0.64 pc. The M_{VMS}/M_{tot} shown here is averaged over five simulations with the same initial conditions and different random seeds. The error bars are the standard deviations calculated from the data and the average value.

(A color version of this figure is available in the online journal.)

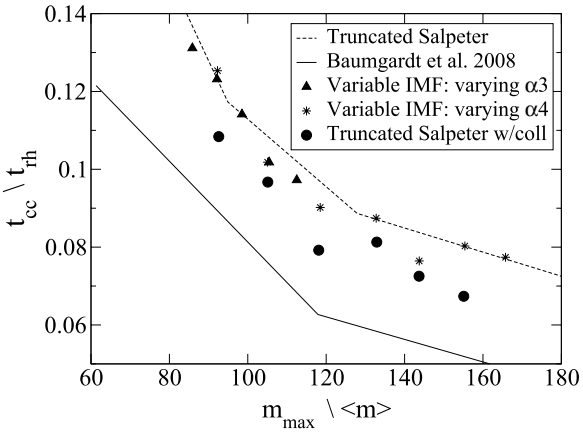

Figure 13. Dependence of the core-collapse time in units of the half-mass relaxation time, on the shape and width of the IMF. The horizontal axis shows the ratio of maximum to mean stellar mass $(m_{max}/\langle m\rangle)$ in the IMF. The solid black line is for mass-segregated clusters (Baumgardt et al. 2008), whereas all other symbols are for unsegregated clusters. The black dashed straight line, the triangles, and the stars denote the simulations with physical stellar collisions turned off whereas the circles represent simulations with collisions (truncated Salpeter IMF with $M_{max} = 110, 100, 90, 80, 70, 60$). The stars correspond to the Variable IMF varied as a power law from -1.72 to -2.3 ($\alpha 4$) and the triangles correspond to the middle section of the Variable IMF varied as a power law from -1.9 to -2.3 ($\alpha 3$). Flatter IMFs (triangles and stars) increase t_{cc} by 30% but when collisions (circles) are included t_{cc} decreases on an average by 15%.

by a factor of ≈10%, implying that σ_c stays almost constant in the core and does not change with S. From this it follows that for $S < 0.15$ both the increase in $\langle m\rangle_c$ as well as ρ_c contribute equally to the decrease in t_{rc}. On the other hand, for larger S, t_{rc} is dominated by $\langle m\rangle_c$ while the contribution from ρ_c is minimal (≈20%). So it is the increase in $\langle m\rangle_c$ that mainly causes the low t_{rc} values for larger S. Thus, the maximum increase in the parameter space for a runaway to occur is driven mainly by "true" primordial mass segregation.

The advantage of including stellar collisions in our code is that we are able to directly determine how much mass eventually ends up in the VMS. Paper I showed that, as the core collapse proceeds, the mass contained in the collapsing core which forms the mass reservoir for the runaway converges to a value $M_{cc} \sim 0.001$–$0.002\ M_{tot}$, where M_{tot} denotes the total mass of the cluster. In general, we find that the fraction of M_{tot} that ends up as a VMS is in a similar mass range as M_{cc} in Paper I. In Figure 12, we show that fraction as a function of S for a cluster with $N = 5 \times 10^5$ stars. It can be clearly seen that the fraction of M_{tot} ending up as a VMS increases almost by a factor of three for $S = 0.3$ and hence mass of the VMS increases significantly with primordial mass segregation. Thus, primordial mass segregation not only increases the parameter space for runaways to occur, but also produces more massive VMS.

3.2. Top-heavy IMFs

As discussed previously, there are indications that some young massive star clusters may be born with IMFs flatter than the Salpeter IMF. Here, we study how such flatter IMFs influence the available parameter space of cluster initial conditions for a runaway to occur. One crucial result from Paper I is that the ratio of maximum to average stellar mass in the IMF is the most important parameter setting the timescale for the onset of core collapse. From Paper I, if $m_{max}/\langle m\rangle < 40$, $t_{cc} \propto (m_{max}/\langle m\rangle)^{-1.3}$, and if $m_{max}/\langle m\rangle \simeq 50$, a domain is reached by any realistic IMF where $t_{cc} \simeq 0.15\, t_{rc}$. A flatter IMF increases the number of massive stars, thus increasing the average stellar mass in the cluster, which in turn causes an increase in t_{cc}. This means that although for flatter IMFs we have more massive stars, the parameter space for runaway collisions to occur actually gets *smaller*. On the other hand, collisions can reduce t_{cc} by constantly dissipating orbital energy (Freitag et al. 2006a). This means that the increase in t_{cc} seen in simulations without an explicit treatment of stellar collisions is to some degree compensated by the effect of collisions. In Figure 13, we quantify this effect for flatter IMFs considering a wide range of $m_{max}/\langle m\rangle$ values. We plot t_{cc}/t_{rh} versus $m_{max}/\langle m\rangle$ with and without collisions. As can be clearly seen, with stellar collisions turned off, t_{cc} increases; but when collisions are included, t_{cc} decreases on average by 15%. Overall this causes t_{cc}/t_{rh} for a collisional cluster causes the core collapse to stay close to the value for the standard Salpeter IMF (0.07) all the way to $m_{max}/\langle m\rangle \approx 140$.

We also studied the combined effects of initial mass segregation and a flat IMF on the evolution of young massive clusters. This is mainly motivated by Espinoza et al. (2009) where the global IMF of the Arches cluster is determined to be flatter than Salpeter, while the Arches is also known to be strongly mass-segregated. Note, however, that the uncertainty on the slope is such that it may not be incompatible with a Salpeter IMF and there are models of the Arches (Harfst et al. 2010) that can explain the degree of mass segregation with a Salpeter IMF and unsegregated initial conditions. On the other hand, Harfst et al. (2010) do not rule out the possibility that Arches could be primordially mass-segregated. In Figure 13, we show the results for primordially mass-segregated clusters using the Baumgardt et al. (2008) recipe, which, unlike the Šubr et al. (2008) recipe, can be applied to clusters with arbitrary density profiles. This way the decrease in t_{cc} is only caused by the increase in the average stellar mass at the center of the cluster. From Figure 13, we see that, as in the unsegregated case, the effect of a flatter IMF increases t_{cc}, and for $m_{max}/\langle m\rangle = 120$ is very close to the standard Salpeter value. The change for $m_{max}/\langle m\rangle = 160$ is only by 20%. Note that $m_{max}/\langle m\rangle = 120$ corresponds to either a Salpeter IMF with a high-mass cutoff at 80 $M_{\odot}$, or to an IMF with a slope of -2.1 and a full mass spectrum (from 0.1 to 120 $M_{\odot}$). This latter slope is precisely the one suggested for the global IMF of the Arches by Espinoza et al. (2009). If the global IMF of the Arches star cluster is also representative of the IMFs for much more massive clusters such as Westerlund 1, this would imply that the simple relation from Paper I can be used to determine whether a young massive cluster will undergo a runaway or not, without explicitly accounting for a different global IMF or primordial mass segregation.

4. SUMMARY AND DISCUSSIONS

This work is a continuation of our study of the runaway collision scenario in young dense star clusters. In this paper, our goal was to investigate the parameter space for runaway collisions to occur, when the effects of stellar collisions, primordial mass segregation, and a globally flatter IMF (as indicated by observations of young massive star clusters) are accounted for. We considered clusters having Plummer density profiles, varying the initial virial radius, the number of stars in the cluster, and the IMF. Primordial mass segregation was generated using the Šubr et al. (2008) and Baumgardt et al. (2008) methods. We naturally expected that primordial mass segregation in a cluster should lead to shorter core-collapse times since the massive stars start their lives closer to the center of the cluster, where the density and therefore collision rates are highest. Indeed, from our simulations we found that the core-collapse time, t_{cc} decreases with increasing the degree of primordial mass segregation, increasing the initial virial radius for runaway collisions to happen, by at least a factor of ≈3.

We find that the simple relation between the core collapse and the central relaxation times ($t_{cc} = 0.15\,t_{rc}$), discussed in Paper I, still holds even with primordial mass segregation. The strong decrease in t_{cc} hence implies a similar reduction in t_{rc}, which accelerates the core collapse and enlarges the parameter space for runaway collisions to occur. This decrease in t_{rc}, in both the Šubr et al. (2008) and Baumgardt et al. (2008) prescriptions, is caused by the strong increase in the average stellar mass in the core. In the Šubr et al. (2008) recipe, the decrease in t_{rc} is also caused by an increase in central density, which, however, does not contribute much at higher degrees of mass segregation ($S > 0.15$).

We find that the fraction of the total cluster mass that is eventually accumulated onto the VMS, the possible progenitor of an IMBH, is comparable to the mass of the collapsing core, M_{cc}, already determined in Paper I. If IMBHs were indeed formed in massive star clusters, our results show that the ratio of the mass of the IMBH to the total stellar cluster mass follows the M/M_{bulge} ratio. However, the runaway collision scenario imposes the requirement that the IMBH must have formed in a cluster with an initial central relaxation time shorter than 20 Myr.

Finally, we find that for top-heavy IMFs (in unsegregated clusters) the parameter space for runaway collisions is *reduced*, since flatter IMFs increase t_{cc} by a factor ≈1.4 for $m_{max}/\langle m\rangle \approx 120$. However, this increase is to some degree balanced by collisions, which happen more frequently in clusters with flatter IMFs as we get more massive stars. In addition, primordial mass segregation in these clusters again reduces t_{cc}, and for an IMF with a slope of -2.1, as may be present in the Arches cluster (Espinoza et al. 2009), this reduced t_{cc} is nearly the same as for an unsegregated cluster with a Salpeter IMF. Thus, if the IMF is Salpeter-like, primordial mass segregation increases the parameter space for runaway collisions to occur, whereas for flatter IMFs the parameter space remains very similar to that in unsegregated clusters with a Salpeter-like IMF. From this we can conclude that if young massive star clusters (like Westerlund 1) are primordially mass-segregated and have an IMF slope similar to the Arches, then the results from Paper I are directly applicable.

We thank John Fregeau and Sourav Chatterjee for the useful discussions. This work was supported by NSF Grant AST-060.7498 and NASA Grant NNX08AG66G at Northwestern University.

REFERENCES

Ardi, E., Baumgardt, H., & Mineshige, S. 2008, ApJ, 682, 1195
Baumgardt, H., De Marchi, G., & Kroupa, P. 2008, ApJ, 685, 247
Baumgardt, H., Makino, J., Hut, P., McMillan, S., & Portegies Zwart, S. 2003, ApJ, 589, L25
Binney, J., & Tremaine, S. (ed.) 1987, Galactic Dynamics (Princeton, NJ: Princeton Univ. Press)
Bolton, C. T. 1972, Nature, 235, 271
Bonnell, I. A., & Bate, M. R. 2006, MNRAS, 370, 488
Bonnell, I. A., & Davies, M. B. 1998, MNRAS, 295, 691
Caputo, F. 1985, Rep. Prog. Phys., 48, 1235
Casares, J. 2007, in IAU Symp. 238, Black Holes from Stars to Galaxies – Across the Range of Masses, ed. V. Karas & G. Matt (Cambridge: Cambridge Univ. Press), 3
D'Amico, N., Possenti, A., Fici, L., et al. 2002, ApJ, 570, L89
de Grijs, R. 1998, MNRAS, 299, 595
Dib, S., Kim, J., & Shadmehri, M. 2007, MNRAS, 381, L40
Elmegreen, B. G. 2004, MNRAS, 354, 367
Espinoza, P., Selman, F. J., & Melnick, J. 2009, A&A, 501, 563
Farrell, S. A., Webb, N. A., Barret, D., Godet, O., & Rodrigues, J. M. 2009, Nature, 460, 73
Ferraro, F. R., Possenti, A., Sabbi, E., et al. 2003, ApJ, 595, 179
Fischer, P., Pryor, C., Murray, S., Mateo, M., & Richtler, T. 1998, AJ, 115, 592
Fregeau, J. M., & Rasio, F. A. 2007, ApJ, 658, 1047
Freitag, M., & Benz, W. 2002, A&A, 394, 345
Freitag, M., Gürkan, M. A., & Rasio, F. A. 2006a, MNRAS, 368, 141
Freitag, M., Rasio, F. A., & Baumgardt, H. 2006b, MNRAS, 368, 121
Gebhardt, K., Rich, R. M., & Ho, L. C. 2002, ApJ, 578, L41
Gebhardt, K., Rich, R. M., & Ho, L. C. 2005, ApJ, 634, 1093
Gerssen, J., van der Marel, R. P., Gebhardt, K., et al. 2002, AJ, 124, 3270
Ghez, A. M., Duchêne, G., Matthews, K., et al. 2003, ApJ, 586, L127
Gill, M., Trenti, M., Miller, M. C., et al. 2008, ApJ, 686, 303

Glebbeek, E., Gaburov, E., de Mink, S. E., Pols, O. R., & Portegies Zwart, S. F. 2009, A&A, 497, 255
Gouliermis, D., Keller, S. C., Kontizas, M., Kontizas, E., & Bellas-Velidis, I. 2004, A&A, 416, 137
Grindlay, J. E., Heinke, C., Edmonds, P. D., & Murray, S. S. 2001, Science, 292, 2290
Gültekin, K., Miller, M. C., & Hamilton, D. P. 2004, ApJ, 616, 221
Gürkan, M. A., Fregeau, J. M., & Rasio, F. A. 2006, ApJ, 640, L39
Gürkan, M. A., Freitag, M., & Rasio, F. A. 2004, ApJ, 604, 632
Harfst, S., Portegies Zwart, S., & Stolte, A. 2010, MNRAS, 409, 628
Heger, A., & Woosley, S. E. 2002, ApJ, 567, 532
Heggie, D., & Hut, P. (ed.) 2003, The Gravitational Million-Body Problem: A Multidisciplinary Approach to Star Cluster Dynamics (Cambridge: Cambridge Univ. Press)
Hénon, M. H. 1971, Ap&SS, 14, 151
Hillenbrand, L. A. 1997, AJ, 113, 1733
Hillenbrand, L. A., & Hartmann, L. W. 1998, ApJ, 492, 540
Kaaret, P., Feng, H., & Gorski, M. 2009, ApJ, 692, 653
Kaaret, P., Prestwich, A. H., Zezas, A., et al. 2001, MNRAS, 321, L29
Kim, S. S., Figer, D. F., Kudritzki, R. P., & Najarro, F. 2006, ApJ, 653, L113
Kormendy, J., & Gebhardt, K. 2001, in AIP Conf. Ser. 586, 20th Texas Symposium on Relativistic Astrophysics, ed. J. C. Wheeler & H. Martel (Melville, NY: AIP), 363
Kroupa, P. 2001, MNRAS, 322, 231
Kroupa, P. 2002, Science, 295, 82
Madau, P., & Rees, M. J. 2001, ApJ, 551, L27
McMillan, S., Vesperini, E., & Portegies Zwart, S. 2008, in IAU Symp. 246, Dynamical Evolution of Dense Stellar Systems, ed. E. Vesperini, M. Giersz, & A. Sills (Cambridge: Cambridge Univ. Press), 41
McMillan, S. L. W., Vesperini, E., & Portegies Zwart, S. F. 2007, ApJ, 655, L45
Merritt, D., & Ferrarese, L. 2001, ApJ, 547, 140
Meynet, G., & Maeder, A. 2000, A&A, 361, 101
Miller, G. E., & Scalo, J. M. 1979, ApJS, 41, 513
Miller, M. C., & Colbert, E. J. M. 2004, Int. J. Mod. Phys. D, 13, 1
Miller, M. C., & Hamilton, D. P. 2002, MNRAS, 330, 232
Mouri, H., & Taniguchi, Y. 2002, ApJ, 566, L17
Murray, S. D., & Lin, D. N. C. 1996, ApJ, 467, 728
Noyola, E., Gebhardt, K., & Bergmann, M. 2008, ApJ, 676, 1008
O'Leary, R. M., O'Shaughnessy, R., & Rasio, F. A. 2007, Phys. Rev. D, 76, 061504
O'Leary, R. M., Rasio, F. A., Fregeau, J. M., Ivanova, N., & O'Shaughnessy, R. 2006, ApJ, 637, 937
Pasquato, M., Trenti, M., De Marchi, G., et al. 2009, ApJ, 699, 1511
Perez Munoz, L. M., & Carpenter, J. M. 2007, BAAS, 38, 879
Portegies Zwart, S. F., Baumgardt, H., Hut, P., Makino, J., & McMillan, S. L. W. 2004, Nature, 428, 724
Portegies Zwart, S. F., Makino, J., McMillan, S. L. W., & Hut, P. 1999, A&A, 348, 117
Portegies Zwart, S. F., & McMillan, S. L. W. 2000, ApJ, 528, L17
Portegies Zwart, S. F., & McMillan, S. L. W. 2002, ApJ, 576, 899
Remillard, R. A., & McClintock, J. E. 2006, ARA&A, 44, 49
Salpeter, E. E. 1955, ApJ, 121, 161
Salpeter, E. E. 1959, ApJ, 129, 608
Sirianni, M., Nota, A., De Marchi, G., Leitherer, C., & Clampin, M. 2002, ApJ, 579, 275
Spitzer, L. (ed.) 1987, Dynamical Evolution of Globular Clusters (Princeton, NJ: Princeton Univ. Press)
Spitzer, L. J. 1969, ApJ, 158, L139
Stolte, A., Brandner, W., Brandl, B., & Zinnecker, H. 2006, AJ, 132, 253
Stolte, A., Grebel, E. K., Brandner, W., & Figer, D. F. 2002, A&A, 394, 459
Šubr, L., Kroupa, P., & Baumgardt, H. 2008, MNRAS, 385, 1673
van der Marel, R. P., Gerssen, J., Guhathakurta, P., Peterson, R. C., & Gebhardt, K. 2002, AJ, 124, 3255
Vishniac, E. T. 1978, ApJ, 223, 986
Watters, W. A., Joshi, K. J., & Rasio, F. A. 2000, ApJ, 539, 331
Webster, B. L., & Murdin, P. 1972, Nature, 235, 37